Solar Energy Materials & Solar Cells 107 (2012) 37–45

Contents lists available at SciVerse ScienceDirect

Solar Energy Materials & Solar Cells

journal homepage: www.elsevier.com/locate/solmat

Modelling of optical durability of enhanced aluminum solar reflectors

Florian Sutter [a,*], Stefan Ziegler [b], Martin Schmücker [c], Peter Heller [a], Robert Pitz-Paal [a]

[a] DLR German Aerospace Center, Institute of Solar Research, Plataforma Solar de Almeria, Ctra. Senés Km. 5, P.O. Box 44, 04200 Tabernas, Almería, Spain
[b] Alanod Aluminium-Veredlung GmbH, Egerstraße 12, D-58256 Ennepetal, Germany
[c] DLR German Aerospace Center, Institute of Materials Research, Linder Höhe, D-51147 Cologne, Germany

ARTICLE INFO

Article history:
Received 27 March 2012
Received in revised form
20 July 2012
Accepted 25 July 2012
Available online 30 August 2012

Keywords:
Aluminum solar reflector
Outdoor weathering
Specular reflectance
Scattering
Localized corrosion of aluminum
Avrami equation

ABSTRACT

In order to reduce electricity generation costs of concentrating solar power (CSP) technologies, new low-cost reflector materials are being developed. These materials need to withstand harsh outdoor conditions without a significant loss in specular reflectance. In this work, samples of enhanced anodized aluminum reflectors protected by a sol–gel coating that have been exposed at different weathering sites were analyzed with an innovative specular reflectometer in order to monitor corrosion and scattering caused by surface roughness. A model to estimate the specular reflectance as a function of exposure conditions at different weathering sites has been developed.

1. Introduction

Aluminum reflectors are increasingly being used in concentrated solar power applications because of their high formability and lightweight properties. They offer flexibility in the design, construction and assembly of new collectors. Because of their high ductility, aluminum mirrors will not break even at high wind loads. The manufacturing process is well suited for mass production because of the coil coating process. Consequently, aluminum reflectors offer a significant cost reduction potential compared to glass mirrors.

Enhanced first-surface aluminum mirrors are produced by anodizing a 0.5 mm-thick polished aluminum substrate. The thickness of the anodized layer is about 3 μm. Afterwards a 65 nm-thick pure aluminum layer is deposited by physical vapor deposition (PVD). The reflectance of the aluminum is enhanced by 1/4wavelength (λ) thick low-index (95 nm SiO_2) and high-index (60 nm TiO_2) refractive oxide coatings. The structure of the SiO_2 and TiO_2 films is known to be columnar and porous [1]. The coating stack is then protected with a (3 μm SiO_2) sol–gel nanocomposite oxide layer (see Figs. 1 and 2).

2. Material and methods

Enhanced aluminum reflector samples have been exposed in Almería and Tabernas (Spain), and in Florida, Golden and Arizona (USA). The degradation mechanism of the outdoor exposed samples has been analyzed with microscopy and with optical measurement devices. Scanning transmission electron microscopy (STEM) has been performed at the National Renewable Energy Laboratory (NREL) with a FEI Tecnai F20 UT in the Z-contrast mode (the intensity is proportional to the atomic number Z) with a high-angle annular dark field (HAADF) detector. Scanning electron microscopy (SEM) has been performed at the materials laboratory of DLR in Cologne with a Carl Zeiss Micro Imaging Ultra 55 FEG. The 2-D light microscope images were made with a Carl Zeiss Axio CSM 700.

The influence of the detected degradation mechanisms on the specular reflectance of the mirror was examined using a prototype of an innovative specular reflectometer. The device enables the measurement of the specular reflectance ρ at different acceptance half-angles φ. The system is based on a photographic method that allows the reflectance characteristics of flat mirrors to be evaluated at any point on its surface. It has a spatial resolution of 37 pixel/mm and a precision of $\pm 0.6\%$ at $\varphi = 12.5$ mrad acceptance half-angle [2]. Herein we denote specular reflectance as ρ ($\lambda = 656$ nm; $\theta = 15^\circ$; $\varphi = 12.5$ mrad) where λ is the wavelength and θ is the angle of incidence.

2.1. Localized corrosion of the aluminum layer

All exposed samples showed localized corrosion spots. The effect was more pronounced at the coastal sites of Almería and Florida but localized corrosion has also been detected at samples exposed in dry desert conditions. Fig. 3 shows a light microscope image of a typical corrosion spot that appeared after 64 months of outdoor exposure in Tabernas.

* Corresponding author. Tel.: +34 950 277 684; fax: +34 950 260 315.
E-mail addresses: Florian.Sutter@dlr.de (F. Sutter), Ziegler@alanod.de (S. Ziegler), Martin.Schmuecker@dlr.de (M. Schmücker), Peter.Heller@dlr.de (P. Heller), Robert.Pitz-Paal@dlr.de (R. Pitz-Paal).

0927-0248/$ - see front matter © 2012 Elsevier B.V. All rights reserved.
http://dx.doi.org/10.1016/j.solmat.2012.07.027

Nomenclature

A_C	area of a single corrosion spot (m^2)
A_{ext}	extended area of all corrosion spots (m^2)
A_{total}	total mirror surface [m^2]
c_J	nucleation rate constant [$s^{-0.5}/mm^2$]
f_C	corroded area fraction (dimensionless)
$f_{C,cont.}$	corroded area fraction for the case of continuous nucleation [dimensionless]
$f_{C,sim.}$	corroded area fraction for the case of simultaneous nucleation (dimensionless)
$f_{ext,cont.}$	extended area fraction for the case of continuous nucleation (dimensionless)
$f_{ext,sim.}$	extended area fraction for the case of simultaneous nucleation (dimensionless)
J	nucleation rate ($s^{-1}\,m^{-2}$)
k	Avrami constant (k is expressed in ($months^{-0.5}$) for an Avrami exponent of $\eta=0.5$) ($s^{-\eta}$)
m	number of dimensions (dimensionless)
m_C	constant (%/months)
m_S	constant (%/months)
N	density of nuclei ($1/m^{-2}$)
n	number of nuclei (dimensionless)
n_{ext}	number of nuclei of extended area (dimensionless)
r	radius of the corrosion spot (m)
r_{eq}	equivalent radius of the corrosion spot (m)
t	time (s)
v_C	growth velocity of a corrosion spot (m/s)
Δt	time interval between the formation of new corrosion spots (s)
$\Delta\rho_C$	specular reflectance loss caused by corrosion ($\lambda=665$ nm; $\theta=15^\circ$; $\varphi=12.5$ mrad) (%)
$\Delta\rho_S$	specular reflectance loss caused by scattering ($\lambda=665$ nm; $\theta=15^\circ$; $\varphi=12.5$ mrad) (%)
η	Avrami exponent (dimensionless)
θ	incidence angle (deg.)
λ	wavelength (nm)
ρ	specular reflectance at wavelength $\lambda=656$ nm, incidence angle $\theta=15^\circ$ and acceptance angle $\varphi=12.5$ mrad (%)
ρ_0	initial specular reflectance before outdoor weathering ($\lambda=665$ nm; $\theta=15^\circ$; $\varphi=12.5$ mrad) (%)
$\rho_{0,fC}$	constant (%)
ρ_{fC}	average specular reflectance of corroded area fraction ($\lambda=665$ nm; $\theta=15^\circ$; $\varphi=12.5$ mrad) (%)
ρ_{fS}	average specular reflectance of non-corroded area fraction ($\lambda=665$ nm; $\theta=15^\circ$; $\varphi=12.5$ mrad) (%)
φ	acceptance angle (mrad)

A STEM cross section image reveals that the degradation occurs at the pure 65 nm-thick aluminum layer (Fig. 4). STEM analysis requires very thin samples that are almost transparent for electrons. Preparation of the 100 Å thick cross section sample was performed by focused ion beam (FIB) to avoid the introduction of defects. Other attempts to prepare the sample (like polishing or grinding) were not successful because the mechanical treatment caused delamination of the sample's coating.

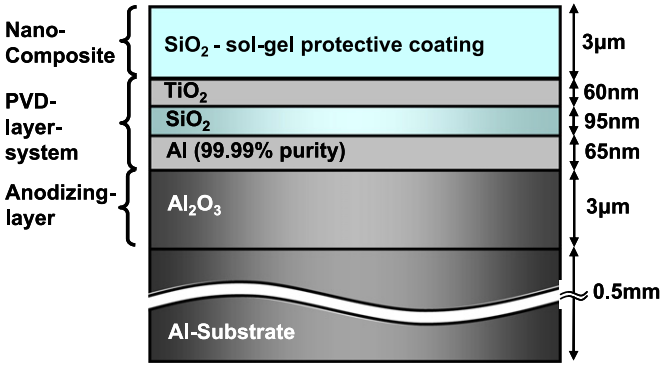

Fig. 1. Schematic composition of enhanced aluminum reflectors.

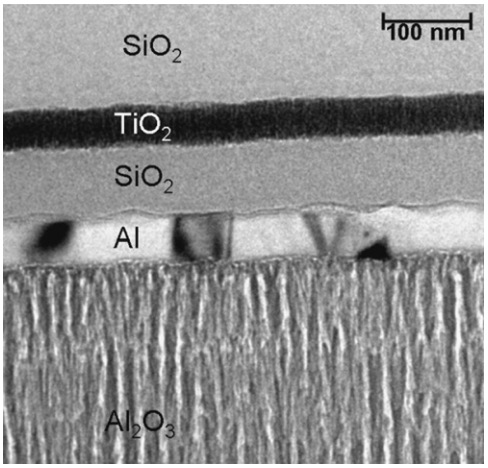

Fig. 2. Cross section viewed in a transmission electron microscope (TEM) .

A vertical energy-dispersive X-ray spectroscopy (EDX) line scan with high spatial resolution detected a loss of the aluminum in the degraded areas (as indicated by the dotted line scan in Fig.4). The left side of the STEM-image shows an unharmed region with an intact pure aluminum layer. This region is probably an "island" (compare Fig. 3).

Further microscopic analysis has shown that the corrosion starts at defects in the 3 µm-thick nanocomposite layer. Fig. 5 shows the corrosion initiation at a coating defect deliberately inserted with a scratching tool as the sample is brought in contact with a sodium chloride solution (50 g/l NaCl in demineralized water).

While the pure aluminum layer corrodes, the SiO_2 and TiO_2 enhancing layers remain almost unharmed. During the corrosion hydrogen bubbles are formed which tend to introduce microcracks or coating break outs in the overlying coatings (see Figs. 3and 5c). The observed corrosion mechanism has similarities with filiform

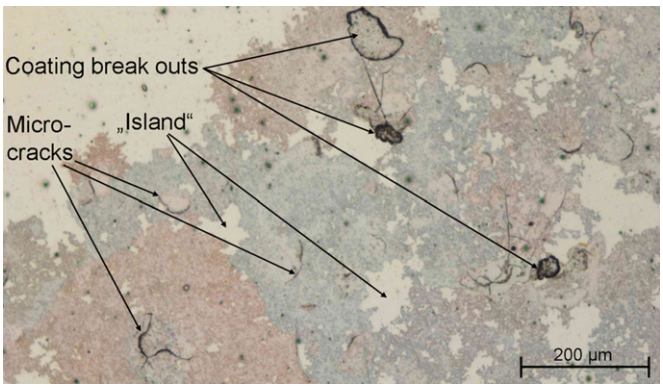

Fig. 3. Typical corrosion of outdoor exposed aluminum reflector samples.